AL-Bahir
Journal for Engineering and Pure Sciences
BJEPS

Manuscript 1125

Fabrication and analysis of Bi_2O_3/Si heterojunction for solar cell applications

Maher Khaleel Ibrahim

Assel Mustafa abdul Majeed

Randa Kamel Husain

Jamal M. Rzaij

ORIGINAL STUDY

Fabrication and Analysis of Bi_2O_3/Si Heterojunction for Solar Cell Applications

Maher K. Ibrahim [a], Assel M.A. Majeed [b], Randa K. Husain [b], Jamal M. Rzaij [a,*]

[a] Department of Physics, College of Science, University of Anbar, Ramadi, Iraq
[b] Department of Physics, College of Science, Mustansiriyah University, Baghdad, Iraq

Abstract

Bismuth oxide (Bi_2O_3) nanoparticles were synthesized via a green route and integrated into Bi_2O_3/Si heterojunction solar cells. Structural analysis confirmed the monoclinic α-Bi_2O_3 phase with a nanoscale crystallite size, while SEM revealed a uniform morphology. Optical studies showed a direct band gap suitable for absorbing visible light. Photoluminescence spectra exhibited dual emissions at 498 nm and 250 nm, attributed to defect states and quantum confinement, highlighting the dual role of Bi_2O_3 as both absorber and transparent window layer. Electrical characterization under dark conditions demonstrated rectifying diode behavior, confirming the formation of a junction. Capacitance−voltage analysis yielded a built-in potential of 0.71 V and a depletion width of 3.66 μm, indicating efficient charge separation. The current-voltage results under illumination indicated an open-circuit voltage of 180 mV, a short-circuit current density of 3.5 μA/cm^2, a fill factor of 14.4 %, and an efficiency of 0.91 %. These results confirm that the interface engineering improves photovoltaic cell performance. They highlight the significant benefits of using environmentally friendly Bi_2O_3/Si heterojunctions.

Keywords: Green synthesis, Bi_2O_3, Nanoparticles, Solar cell, Heterojunctions

1. Introduction

The effects of climate change and the global energy crisis are mitigatable by considering more research on renewable energy technologies. Hence, photovoltaic solar energy systems can be identified as one of the most valid and long-term remedies to the problem of not being dependent on fossil fuels, and they also help decrease the level of greenhouse gas emissions. The efficiency, effectiveness, and cost of photovoltaic devices however are still critical issues that need to be addressed to allow the large-scale application of these technology [1]. The photovoltaic energy market has the largest number of solar cells made of silicon. This is attributed to their stability and high level of manufacturing procedures. Nevertheless, the conventional silicon cells are limited to heat loss as well as charge-carrier recombination which decreases its efficiency to its theoretical point. To address these issues, heterojunction structures have been proposed as a viable solution, offering improved light absorption, charge-carrier transport, and reduced recombination process [2−5].

Because bismuth oxide (Bi_2O_3) (an n-type semiconductor with a wide band gap (~3.2 electron volts)) is very suitable for photovoltaic applications, such as photocatalysis, gas sensing, and solar energy conversion, it has received considerable attention. [6−9]. Its unique electronic structure, resulting from the contributions of Bi 6s and 6p orbitals in the valence band, allows for favorable band alignment when combined with silicon [10,11]. Thin films can also be manufactured from bismuth oxide (Bi_2O_3) using environmentally friendly methods, where plant extracts act as reducing and stabilizing agents. Besides enhancing the optical and structural properties of the resulting

Received 2 November 2025; revised 14 January 2026; accepted 19 January 2026.
Available online 27 March 2026

* Corresponding author.
E-mail addresses: mkibrahim@uoanbar.edu.iq (M.K. Ibrahim), aseelalaziz@uomustansiriyah.edu.iq1 (A.M.A. Majeed), dr.randa.kamel@uomustansiriyah.edu.iq (R.K. Husain), sc.jam72al@uoanbar.edu.iq (J.M. Rzaij).

https://doi.org/10.55810/2313-0083.1125

films, this approach does not diminish the environmental impact of nanomaterial manufacturing. Compared to other traditional chemical methods, the green synthesis of bismuth oxide nanoparticles is attracting considerable attention due to its high efficiency and ease of preparation [12]. Using environmentally friendly methods to manufacture thin films from bismuth oxide (Bi_2O_3) provides a significant economic advantage, in addition to its favorable photovoltaic properties. [13–15]. Using plant extracts as reducing and stabilizing agents eliminates the need for chemicals due to the high cost and risks associated with these materials, which in turn leads to a reduction in production costs. The simple distillation deposition process on silicon substrates requires minimal equipment and energy consumption compared to traditional manufacturing techniques [16,17]. It is evident from the above that all these factors and advantages combined highlight the potential of Bi_2O_3/Si heterojunction solar cells and are considered a suitable option for cost reduction and scalability for renewable energy applications [18–20].

By adjusting the band gap and controlling the thickness, Bi_2O_3/Si heterojunctions have achieved improved photovoltaic performance, as demonstrated by recent studies. Nevertheless, systematic investigations into green-synthesized Bi_2O_3 thin films for solar cell applications remain limited. Therefore, the present work focuses on the eco-friendly fabrication of Bi_2O_3 nanoparticles using lemon leaf extract and their integration into n-Si heterojunction solar cells. Structural, optical, and electrical characterizations are performed to assess the potential of this low-cost nanosystem as a candidate for efficient and sustainable photovoltaic devices.

Nomenclature

V_{oc}	Open-circuit voltage (V)
J_{sc}	Short-circuit current density (mA/cm^2)
FF	Fill factor (%)
η	Power conversion efficiency (%)
Eg	Band gap energy (eV)
PL	Photoluminescence
SEM	Scanning Electron Microscopy
XRD	X-ray Diffraction
C–V	Capacitance–Voltage analysis
I–V	Current–Voltage characteristics
hkl	Miller indices (crystallographic planes)
Cu Kα	Copper K-alpha radiation line (Å)
W	Depletion width (μm)
V_{bi}	Built-in potential (V)
n-Si	n-type Silicon substrate
α-Bi_2O_3	Monoclinic alpha phase of Bismuth Oxide
NaOH	Sodium Hydroxide
pH	Acidity/basicity of solution

2. Materials and methods

2.1. Substrate preparation

In this work, silicon and quartz deposition substrates were used for depositing the Bi_2O_3 solar cell film. To eliminate surface impurities, the substrates were first cleaned using ethanol and ultrasonic baths, followed by rinsing with distilled water. Highly reflective n-type silicon substrates (1 cm^2) with a resistivity between 0.5 and 2.5 Ω cm were used, and (111) crystal orientation was used in this study.

2.2. Eco-friendly preparation of a reducing and stabilizing agent for nanomaterial synthesis

Lemon leaves were obtained from a local market in Baghdad, then finely chopped and rinsed with distilled water to eliminate contaminants. Separately, 35 g of Lemon plant were combined with 100 mL of distilled water and subjected to homogenization with continuous stirring at 120 °C. After cooling, the mixture was filtered to obtain a Lemon plant extract, which was subsequently utilized as a reducing and stabilizing agent for the synthesis of Bi_2O_3 nanoparticles.

2.3. Fabrication of Bi_2O_3 nanoparticles

To synthesize Bi_2O_3 nanoparticles, 30 mL of freshly prepared Lemon plant extract was added to a 0.1 M solution of bismuth nitrate pentahydrate, $Bi(NO_3)_3 \cdot 5H_2O$, supplied by Reagent World, USA, with purity of 99.99 %. The pH of the mixture was adjusted to 6–7 by the dropwise addition of a 0.1 M Sodium hydroxide (NaOH, Merck, Germany, with purity greater than 99 %) solution under continuous stirring. To form the precipitate, the solution was heated to 80 °C, after which the temperature was reduced to 60 °C and maintained at this level for 80 min. The mixture was left at room temperature (26 °C) overnight, after which it underwent a solid product separation process using a centrifuge (Eppendorf 5810R, Germany) at a speed of 14,000 rpm for 22 min. To remove any remaining reactants and impurities, the resulting precipitate was thoroughly washed using distilled water and absolute ethanol (C_2H_5OH), supplied by the German company Merck, with a purity of over 99.5 %. Using a drying oven and at a temperature of 550 °C for 4 h, the precipitate was dried, after which it was ground into a fine powder and subjected to analysis. Plant extracts were used as an

environmentally friendly reducing agent in the synthesis of bismuth oxide (Bi_2O_3). Mixing them with bismuth nitrate resulted in a color change from yellow to white, indicating the formation of bismuth oxide nanoparticles. Fig. 1 illustrates the green synthesis process as a schematic model.

For the deposited Bi_2O_3 nanoparticle films, their structural properties were analyzed using an X-ray diffraction spectrometer (Shimadzu-6000, Japan) operating at 40 kV and 30 mA, with a scanning rate of 5°/minute. The optical properties were evaluated using an ultraviolet-visible spectrometer (Lasany LI-2800, India). The surface morphology and nanostructure of the Bi_2O_3 film were examined using a field emission scanning electron microscope (ZEISS EM-3200, Germany). Photoluminescence (PL) measurements of the Bi_2O_3 nanoparticles were carried out using a PerkinElmer LS 55 luminescence spectrophotometer (PerkinElmer, USA), with slit widths of 5 nm, integration time of 0.5 s, and an excitation wavelength of 330 nm. Using specially designed masks, aluminum (Al) films were deposited on the rear side of the n-type silicon substrate and on the surface of the Bi_2O_3 nanoparticle film to form ohmic contacts. A schematic representation of the Bi_2O_3 NPs/NPs/n-Si-based solar cell structure is shown in Fig. 2.

I–V measurements were conducted at room temperature under both dark and illuminated conditions using a controlled DC power source and an electrometer. The solar cell performance was evaluated using a monochromator system, calibrated against a standard silicon power meter for accurate measurements of light intensity.

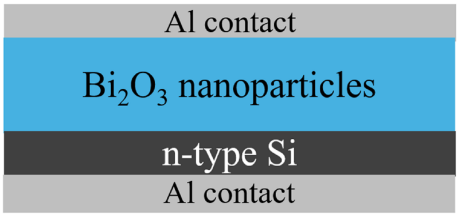

Fig. 2. Cross-sectional schematic of the Bi_2O_3/Si heterojunction solar cell structure with Al contacts deposited by thermal evaporation.

3. Result and discussion

The structural characteristics of Bi_2O_3 nanoparticles synthesized using lemon extract are presented in the XRD pattern of Fig. 3. The observed Bragg diffraction peaks correspond to the crystal planes (102), (221), (311), (400), (222), (122), (412), (321), (242), (232), (800), and (802), confirming the formation of a monoclinic α-Bi_2O_3, matched well with the standard Pdf card No.41-1449. The average crystallite size (D) of the deposited film has been estimated using the Scherrer formula (Equation (1)) [21,22].

$$D = \frac{k\lambda}{\beta \cos\theta} \quad (1)$$

where k is about 0.9 (shape factor), λ is the wavelength of X-ray for Cu Kα = 1.54 Å, and θ is the

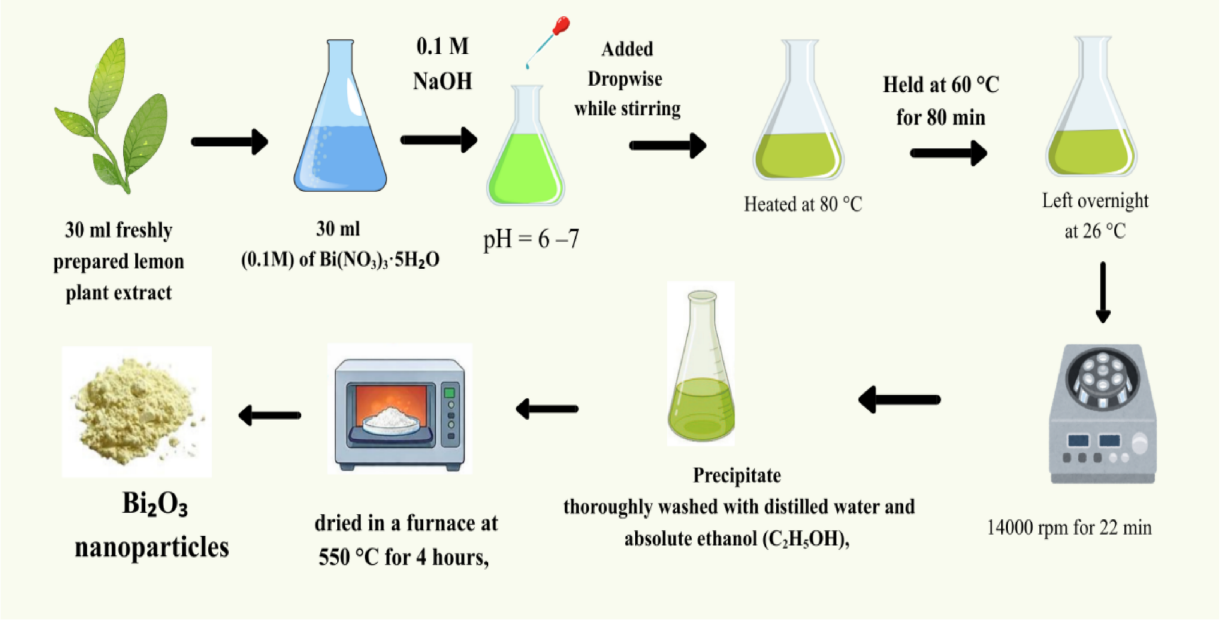

Fig. 1. Schematic illustration of the green synthesis of Bi_2O_3 nanoparticles using lemon leaf extract.

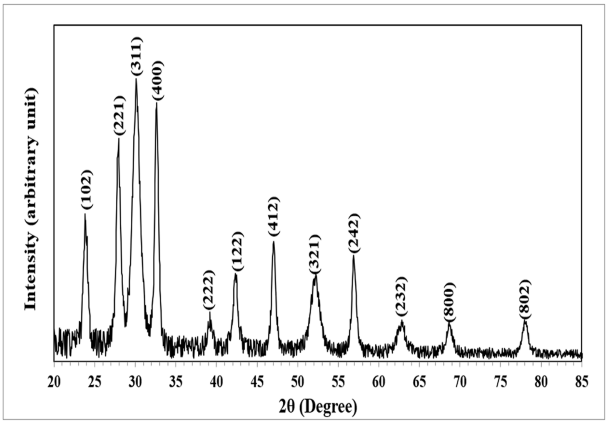

Fig. 3. XRD spectrum of Bi_2O_3 thin film synthesized using lemon extract.

diffraction angle. The calculated average crystallite size corresponding to the (311) dominant diffraction peak was approximately 7.6 nm, as listed in Table 1.

Such nanoscale dimensions enhance quantum confinement effects, resulting in a widened band gap compared to the bulk Bi_2O_3. Similar size-dependent band-gap widening has been reported in green-synthesized Bi_2O_3 nanoparticles prepared using *Mentha pulegium* extract by *Motakef-Kazemi et al.* [19], which supports the present findings.

The FE-SEM analysis (Fig. 4) revealed irregular nanoscale morphology with enhanced surface roughness, and the particle size distribution ranged between 3 and 43 nm with an average particle size of ~10 nm.

This distribution indicates the regular formation and growth of Bi_2O_3 nanoparticles, which in turn increases the effective surface area of the membrane. For photovoltaic cell applications, this morphological feature is very useful, as it promotes stronger light-matter interaction, facilitates charge separation at the Bi_2O_3/Si interface, and helps reduce recombination losses, which in turn supports the overall performance of heterojunction solar cells [23].

Table 1. XRD parameter for the synthesized Bi_2O_3 thin film solar cell.

2θ (deg)	FWHM	Int%	d_{hkl} (Å)	D (nm)	Miller Indices (hkl)
23.877	0.591	48	3.724	13.8	(102)
27.916	0.590	76	3.194	13.9	(221)
30.112	1.085	100	2.965	7.6	(311)
32.624	0.517	95	2.743	16.0	(400)
39.175	0.664	11	2.298	12.7	(222)
42.336	0.737	27	2.133	11.6	(122)
47.049	0.591	40	1.930	14.7	(412)
52.148	1.254	28	1.753	7.1	(321)
56.938	0.590	36	1.616	15.3	(242)
62.784	1.107	11	1.479	8.4	(232)
68.687	0.886	10	1.365	10.9	(800)
78.055	0.811	13	1.223	12.6	(802)

Energy-dispersive X-ray spectroscopy (EDS) analysis can reveal the fabricated Bi_2O_3 nanostructure from Fig. 5. It is also possible to conclude from the EDX spectrum that only bismuth and oxygen are present. This shape leads to an increase in the effective surface area, which in turn enhances photon absorption and facilitates charge separation at the Bi_2O_3/Si interface. The purity of the composition reduces defect-related recombination, consistent with reports by *Ascencio Aguirre and Herrera Becerra* [24], who observed similar clean Bi_2O_3 phases synthesized via tannic acid-assisted methods.

Fig. 6 displays the optical transmittance spectrum of the Bi_2O_3 nanoparticle film coated on a quartz substrate. The Bi_2O_3 nanoparticle film exhibited an optical transmittance of approximately 90% at wavelengths ranging from 500 to 1000 nm, while it decreased between 200 and 500 nm. The transmittance reduction in this wavelength range can be attributed to the high concentration of free electrons at these wavelengths [25]. The energy gap (Eg) of the Bi_2O_3 nanoparticle film was calculated for the direct transition by plotting $(\alpha h\nu)^2$ against photon energy ($h\nu$), as shown in Fig. 6b. In this case, α stands for the absorption coefficient. Using Equation (2), the energy gap can be estimated by extending the straight part of the plot to the photon energy axis [26].

$$(\alpha h\nu)^2 = A(h\nu - Eg) \tag{2}$$

Where α is the absorption coefficient, h is Blank constant, ν is the frequency of the incident photon, and Eg is the energy gap.

The direct Eg of the Bi_2O_3 nanoparticle film was found to be 3.62 eV. This value is larger than the bulk Bi_2O_3 band gap (~3.2 eV), which can be attributed to quantum confinement in nanocrystals. Comparable band-gap widening effects were reported by *Kumari et al.* [27] in Bi_2O_3 nanostructures prepared by pulsed laser deposition, highlighting the consistency of the present results.

The room-temperature photoluminescence (PL) spectra of Bi_2O_3 nanoparticles, excited at a wavelength of 330 nm, are shown in Fig. 7, exhibiting two distinct emission features. The first visible emission peak appeared at 498 nm (2.48 eV), which can be attributed to intrinsic defects such as oxygen vacancies and interstitials. These defect states act as centers for radiative recombination, which in turn leads to the introduction of intermediate energy levels that enhance light absorption. *Oudghiri*

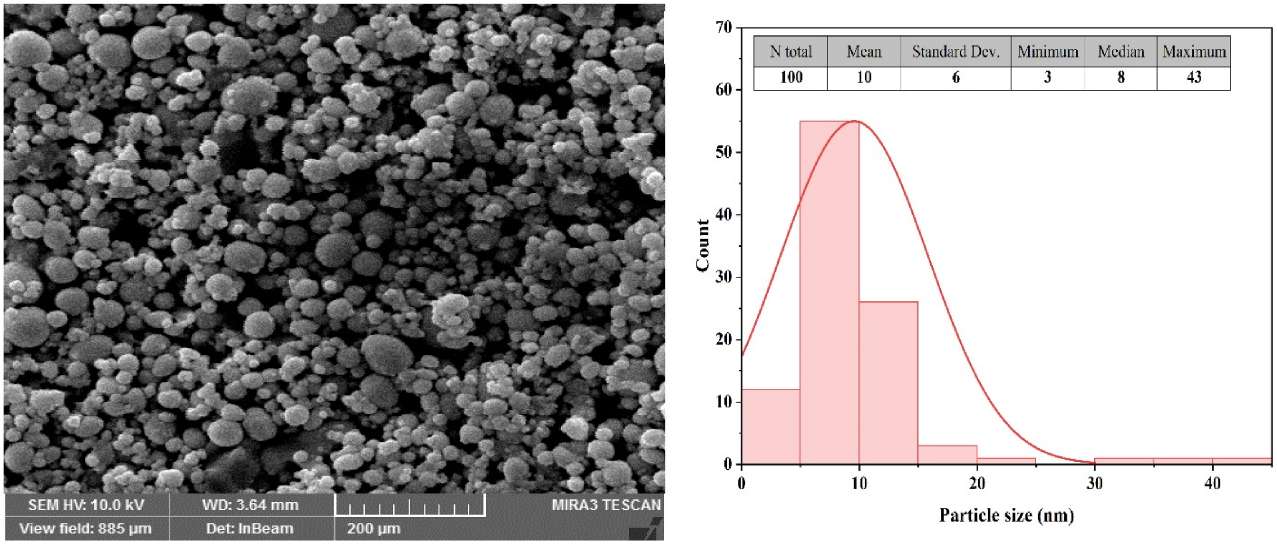

Fig. 4. FE-SEM micrograph images of Bismuth oxide nanoparticles synthesized using lemon extract.

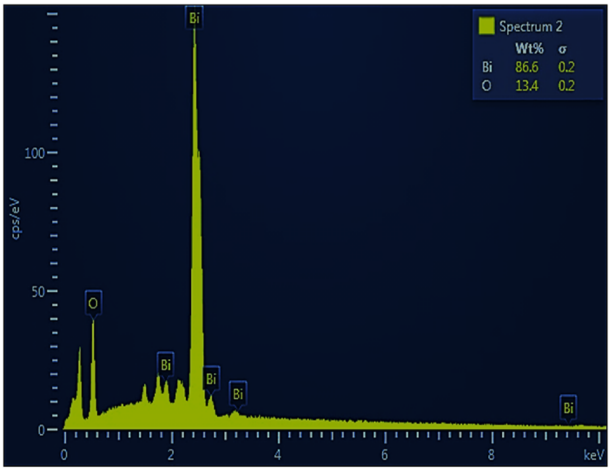

Fig. 5. EDX spectrum of Bi_2O_3 nanomaterial confirming Bi and O composition.

Hassani et al. [28]. This confirms its role in improving the performance of photovoltaic cells, and similar emissions have been reported to be associated with defects in α-Bi_2O_3 nanoparticles.

It was observed that the peak of ultraviolet emission was at 250 nm (~4.96 eV), which is attributed to quantum confinement effects and high-energy transitions involving defect-related states. Although the ultraviolet emission lies outside the main solar spectrum, the existence of such emission confirms the ability of Bi_2O_3 nanoparticles to maintain high-energy electronic transitions. These emissions combined highlight the dual role of Bi_2O_3: its absorption of visible light through defects, which promotes charge separation, as well as its transparency to ultraviolet radiation, allowing bismuth oxide to act as a permeable layer in the Bi_2O_3/Si heterojunction. In photovoltaic cell applications,

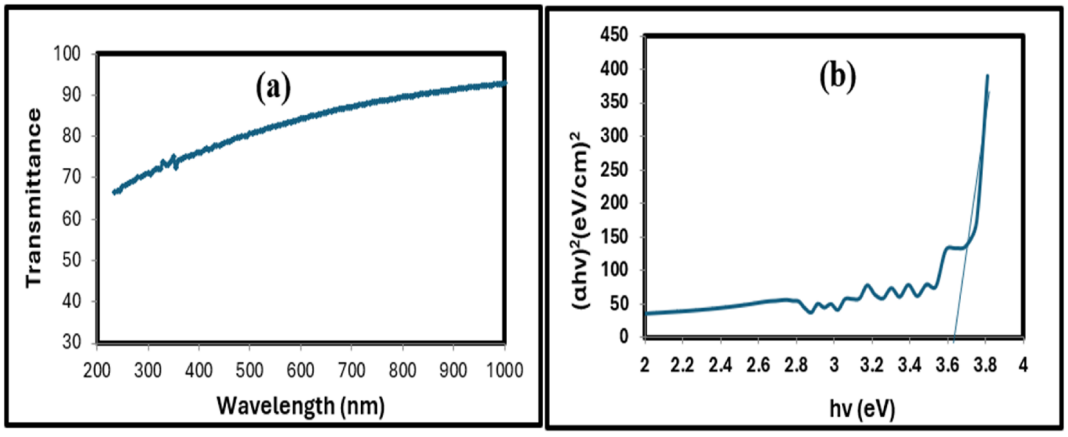

Fig. 6. UV–Vis analysis of Bi_2O_3 thin films (a) optical transmittance (b) $(\alpha h\nu)^2$ versus photon energy plot.

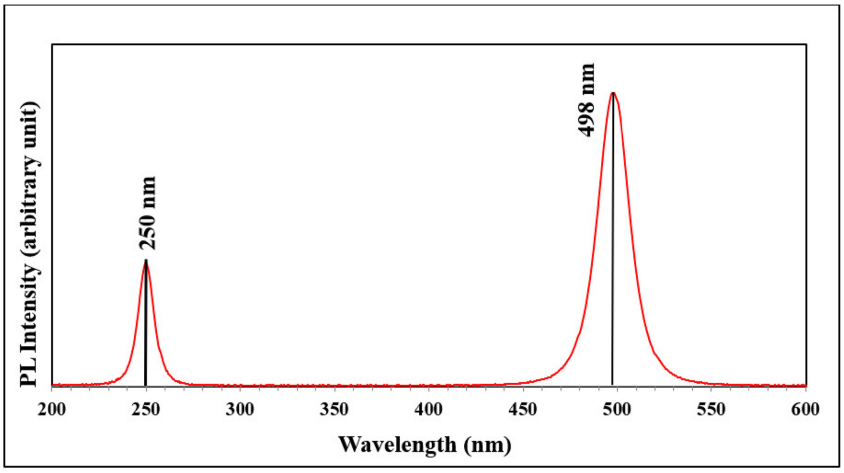

Fig. 7. Room temperature photoluminescence spectra of Bi_2O_3 thin film excited at 330 nm.

these properties are extremely useful, indicating the potential for improving the properties of these cells for manufactured membranes through defect engineering and size control.

The current-voltage density (*J-V*) characteristics of the Bi_2O_3/Si heterojunction at room temperature and under dark conditions show clear rectification behavior typical of a diode, as illustrated in Fig. 8. What confirms the success of forming a functional heterojunction between Bi_2O_3 and Si is that the forward bias region shows a sharp increase in current density, while the reverse bias remains almost constant with a negligible leakage current.

The partial saturation observed at higher forward voltages also indicates the presence of series resistance, which limits the transfer of charge carriers. Series resistance was identified as a limiting factor of efficiency by reporting similar rectification behavior in thermally oxidized Bi_2O_3/Si junctions [29].

The capacitance–voltage (*C–V*) analysis provides further insight into the junction properties. *C–V* curve of the Bi_2O_3/Si heterojunction is illustrated in Fig. 9. The linear relationship between $1/C^2$ and the applied bias allowed for the extraction of an internal voltage (V_{bi}) of 0.71 V and a drain width (W) of 3.66 μm. These values confirm the presence of a strong internal electric field that facilitates charge separation across the junction. The relatively wide depletion region is consistent with the resistivity of the silicon substrate and supports photovoltaic operation. Comparable *C–V* analyses in SnO_2/Si heterojunctions demonstrated that wide depletion widths enhance carrier separation but limit current density if series resistance is high [30,31].

The illuminated J–V curve of the Bi_2O_3/Si solar cell, shown in Fig. 10, consolidates the photovoltaic performance of the device. The extracted parameters were an open-circuit voltage (V_{Oc}) of 180 mV, a

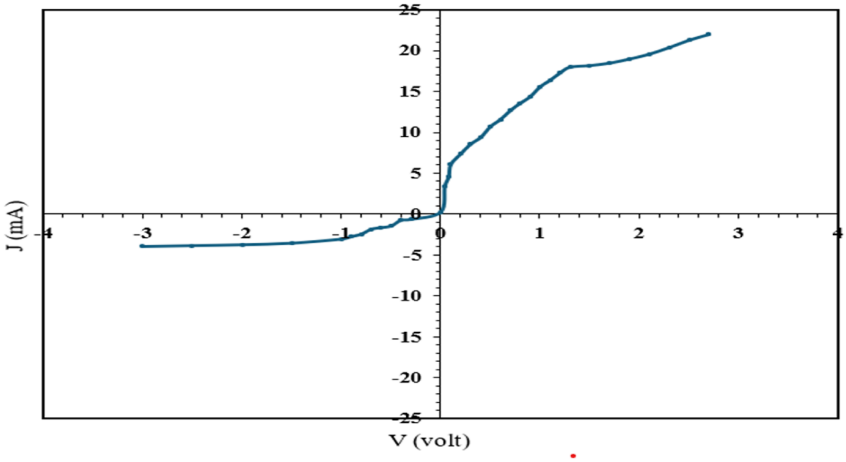

Fig. 8. Current density–voltage (J–V) characteristics of Bi_2O_3/Si heterojunction under dark conditions at room temperature.

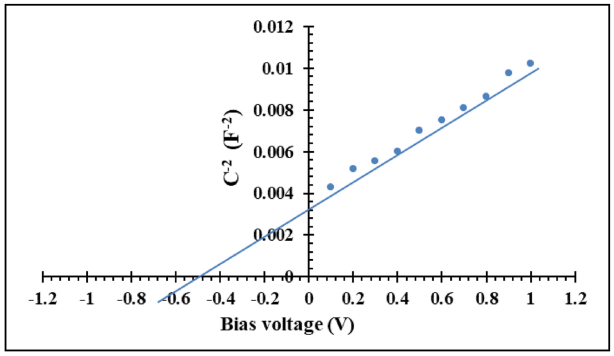

Fig. 9. Capacitance–voltage analysis parameters of Bi_2O_3/Si heterojunction. The plot of $1/C^2$ versus applied bias is shown, where the y-axis corresponds to in units of F^{-2} (normalized to junction area, yielding cm^4/F^2). This representation enables the extraction of the built-in potential (V_{bi}) and depletion width (W) from the linear region of the curve.

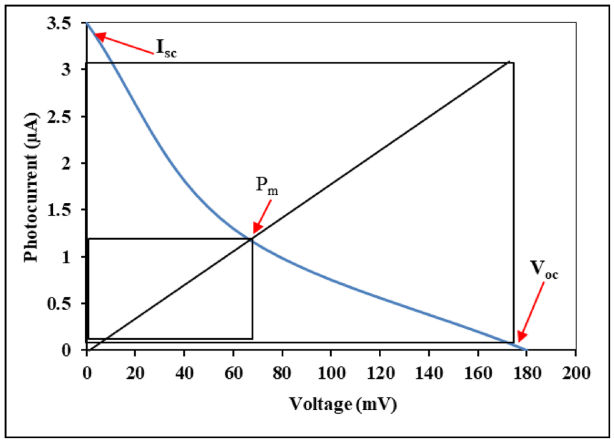

Fig. 10. Current density–voltage (J–V) curve under illumination showing V_{oc}, J_{sc}, FF, and efficiency of Bi_2O_3/Si solar cell.

short-circuit current density (J_{Sc}) of 3.5 μA/cm^2, a maximum voltage (V_{max}) of 70 mV, and a maximum current (I_{max}) of 1.3 μA/cm^2. Using Equations (3) and (4), the fill factor (*FF*) was calculated as 14.4% and the conversion efficiency (η) as 0.91%. The modest efficiency is attributed to series resistance and interface recombination, which is consistent with the dark *J–V* behavior shown in Fig. 8.

$$FF = \frac{I_{max}\, V_{max}}{I_{Sc}\, V_{Oc}} \tag{3}$$

$$\eta = \frac{I_{max}\, V_{max.}}{P_{in}} \times 100\% \tag{4}$$

These results align with previous reports on biosynthesized Bi_2O_3/Si heterojunctions, which also demonstrated low efficiencies but highlighted the potential of interface engineering and doping strategies to improve performance [19].

The comparative table (Table 2) highlights the synthesis routes and photovoltaic outcomes of Bi_2O_3-based systems reported in the literature alongside the present work. Recent studies, such as those by Motakef-Kazemi et al. [19], Ascencio Aguirre & Herrera Becerra [24], and Oudghiri-Hassani et al. [28], primarily focused on the green or sol–gel synthesis of Bi_2O_3 nanoparticles for photocatalytic applications, without reporting photovoltaic parameters. More recent work by *Abd* [31] demonstrated the feasibility of a biosynthesized Bi_2O_3/Si solar cell, achieving an open-circuit voltage of 200 mV, a short-circuit current density of 4 μA/cm^2, and an efficiency close to 1%.

In comparison, the present study using lemon leaf extract achieved V_{oc} = 180 mV, J_{sc} 3.5 = 3.5 μA/cm^2, and η = 0.91%. These values are consistent with what Abd [21] stated, meaning that green synthesis methods can be replicated while emphasizing the ongoing limitations of low current density and efficiency. By comparison, it becomes clear that while green synthesis methods are environmentally attractive and reproducible, further improvement in interface quality, film thickness and defect control is necessary to upgrade heterogeneous Bi_2O_3/Si junctions from proof-of-concept devices to practical photovoltaic applications.

4. Conclusions, limitations, and future recommendations

This work demonstrates the feasibility of successfully integrating environmentally friendly, industrially manufactured bismuth oxide (Bi_2O_3) molecules into bismuth oxide/silicon (Bi_2O_3/Si) heterojunctions. Optical, electrical, and structural analyses confirmed the formation of a functional junction, while photoluminescence spectra revealed defect-related emissions. Capacitance and potential

Table 2. Bi_2O_3 manufacturing methods and photovoltaic cell performance in previous studies: a summary and comparison with current work.

Synthesis Route	Device Type	V_{oc} (mV)	J_{sc} (μA/cm^2)	η	Reference
Green synthesis (Mentha extract)	Material only (no PV)	–	–	–	[19]
Tannic acid-assisted	Bi_2O_3 nanoparticles (photocatalysis)	–	–	–	[24]
Sol–gel	Bi_2O_3 NPs (photocatalysis)	–	–	–	[28]
Biosynthesis (plant extract)	Bi_2O_3/Si solar cell	200	4	~1%	[31]
Lemon leaf extract (green synthesis)	Bi_2O_3/Si solar cell	180	3.5	0.91%	**Present work**

analysis indicated the presence of a strong internal potential. What confirms the validity of the concept of environmentally friendly Bi_2O_3/Si solar cells is the illuminated J-V curve provided as quantitative evidence.

Despite the above, there are still major limitations that restrict the device's efficiency. These limitations are as follows:

- Series resistance within the heterojunction reduces the fill factor.
- Interface recombination at the Bi_2O_3/Si boundary lowers current density.
- Restricted spectral response, with weak absorption beyond the visible range.
- Low photocurrent output is insufficient for practical applications.

Future research should therefore prioritize:
Interface engineering (surface passivation, doping, or buffer layers) to suppress recombination.

- Optimization of film thickness and crystallinity to minimize resistive losses.
- Advanced deposition techniques for uniform coverage and improved contact quality.
- Hybrid or tandem architectures combining Bi_2O_3 with complementary semiconductors to extend spectral absorption.
- To assess the possibility of reproducibility and long-term stability under operatin conditions, scalability studies are conducted.

Therefore, by addressing the aforementioned limitations and obstacles, Bi_2O_3/Si heterojunctions can be developed and transformed from prototypes into viable and sustainable photovoltaic devices.

Source of Funding

This research did not receive any specific grant from funding agencies in the public, commercial, or not-for-profit sectors.

Conflict of interest

None declared.

Ethical Approval

This study did not use human subjects or animals in this work.

Data availability

The data supporting the findings of this study are available upon request from the corresponding author.

Author Contributions

Assel Mustafa abdul Majeed emphasized numerical computations. Randa Kamel Husain and Maher Khaleel Ibrahim analyzed the data. Jamal M. Rzaij proposed and supervised the project. All authors contributed to the composition of the text and agreed to its publication.

References

[1] Ghosh BK, Weoi CNJ, Islam A, Ghosh SK. Recent progress in Si hetero-junction solar cell: a comprehensive review. Renew Sustain Energy Rev 2018;82:1990–2004. https://doi.org/10.1016/j.rser.2017.07.022.
[2] Abdulrahman A, Alanazi AK, Alsalmah HA, Mubeen S, Elboughdiri N, Jery AEL, et al. Insights into the development of visible-light-induced CeO_2-TiO_2/g-C_3N_4 heterojunction catalysts for the mitigation of antibiotic pollutants. J Water Process Eng 2025;76:108293. https://doi.org/10.1016/j.jwpe.2025.108293.
[3] Alharbi FH, Kais S. Theoretical limits of photovoltaics efficiency and possible improvements by intuitive approaches learned from photosynthesis and quantum coherence. Renew Sustain Energy Rev 2015;43:1073–89. https://doi.org/10.1016/j.rser.2014.11.101.
[4] Khalefa AA, Marei JM, Radwan HA, Rzaij JM. In2O3-CuO nano-flakes prepared by spray pyrolysis for gas sensing application. Dig J Nanomater Biostruct 2021;16:197–204. https://doi.org/10.15251/DJNB.2021.161.197.
[5] Ali IM, Rzaij JM, Abbas QA, Ibrahim IM, Alatta HJ. Structural, optical and sensing behavior of neodymium-doped vanadium pentoxide thin films. Iran J Sci Technol Trans A Sci 2018;42:2375–86. https://doi.org/10.1007/s40995-018-0553-5.
[6] Ghdeeb NJ, Abdul Majeed AM, Mohammed AH. Antibacterial activity and physical properties of some metal oxide nanoparticles prepared by different methods. AIP Conf Proc 2023;2834. https://doi.org/10.1063/5.0161636.
[7] Tran QP, Fang JS, Chin TS. Properties of fluorine-doped SnO2 thin films by a green sol-gel method. Mater Sci Semicond Process 2015;40:664–9. https://doi.org/10.1016/j.mssp.2015.07.047.
[8] Ismail RA, Al-Naimi A, Al-Ani AA. Studies on fabrication and characterization of a high-performance Al-doped ZnO/n-Si (1 1 1) heterojunction photodetector. Semicond Sci Technol 2008;23. https://doi.org/10.1088/0268-1242/23/7/075030.
[9] Ghdeeb NJ, AbdulMajeed AM, Mohammed AH. Role of extracted nano-metal oxides from factory wastes in medical applications. Iraqi J Sci 2023;64:1704–16. https://doi.org/10.24996/ijs.2023.64.4.12.
[10] Rzaij JM, Abbas QA, Khalaf AM. Investigating the structural, topographical, morphological and optical effects of AgO on sprayed SnO2 thin films. Bull Mater Sci 2023;46:200. https://doi.org/10.1007/s12034-023-03040-z.
[11] Ibraheam AS, Rzaij JM, Arshad MKM. Influence of magnesium content on the structural, optical, and electrical properties of Cu2(Zn1-xMgx)SnS4 nanostructured Quaternary thin film synthesized using the sol–gel method. J Electron Mater 2023;52:414–21. https://doi.org/10.1007/s11664-022-10002-4.
[12] Shamshuddin M, Abderrahmane A, Koulali A, Eid MR, Shahzad F, Jamshed W. Thermal and solutal performance of Cu/CuO nanoparticles on a non-linear radially stretching surface with heat source/sink and varying chemical reaction effects. Int Commun Heat Mass Tran 2021;129:105710. https://doi.org/10.1016/j.icheatmasstransfer.2021.105710.
[13] Ahmed RS, Mohammed RS, Abdul Majeed AM, Sudhakaran A. Biological activity of MgO nanoparticle synthesis by plasma-assisted reduction method. Phys

Scripta 2024;99:115901. https://doi.org/10.1088/1402-4896/ad7dbc.
[14] Nazari P, Faramarzi MA, Sepehrizadeh Z, Mofid MR, Bazaz RD, Shahverdi AR. Biosynthesis of bismuth nanoparticles using Serratia marcescens isolated from the Caspian Sea and their characterisation. IET Nanobiotechnol 2012;6:58–62. https://doi.org/10.1049/iet-nbt.2010.0043.
[15] Tavakoli F, Salavati-Niasari M, Badiei A, Mohandes F. Green synthesis and characterization of graphene nanosheets. Mater Res Bull 2015;63:51–7. https://doi.org/10.1016/j.materresbull.2014.11.045.
[16] Gür M, Gürgenç E, Coşanay H, Öztop HF. Novel nano-Y2O3/myristic acid nanocomposite PCM for cooling performances of electronic device with various fin designs. J Energy Storage 2024;100:113646. https://doi.org/10.1016/j.est.2024.113646.
[17] Radwan HA, Marei JM, Khalefa AA, Rzaij JM. ZnO/PSi nanoparticles thin film for NO2 sensing application prepared by pulsed laser deposition. Indian J Phys 2024;98:455–67. https://doi.org/10.1007/s12648-023-02806-9.
[18] Amari A, Sultan Aljibori HS, Ismail MA, Diab MA, El-Sabban HA, Umarov A, et al. Engineering novel 2D MXene-based dual Z-scheme heterojunction photocatalyst for enhanced TC hydrochloride degradation and hydrogen evolution. J Water Process Eng 2025;70:107127. https://doi.org/10.1016/j.jwpe.2025.107127.
[19] Motakef-Kazemi N, Yaqoubi M. Green synthesis and characterization of bismuth oxide nanoparticle using mentha pulegium extract. Iran J Pharm Res 2020;19:70–9. https://doi.org/10.22037/ijpr.2019.15578.13190.
[20] Zain Alaabedin AA, Abdul Majeed AM, Hamza BH. Green synthesis of silver nanoparticles and their effect on the skin determined using IR thermography. Kuwait J Sci 2024;51:100076. https://doi.org/10.1016/j.kjs.2023.07.002.
[21] Modhi MK, Rzaij JM. Synthesis and characterization study of CuO thin film and CuO-CeO2 nanostructured composite using chemical spray pyrolysis. In: Al-kadhum 2nd international conference on modern applications of information and communication technology. Baghdad, Iraq: AIP Conference Proceedings; 2023.
[22] Mohammed Enad A, Rzaij JM. Synthesis of CuO thin film incorporated with nanostructured Nd2O3 deposited by pulsed laser deposition for ammonia sensing applications. Nano 2025;20. https://doi.org/10.1142/S1793292024501133.
[23] Rzaij JM, Marei JM, Ibrahim MK, Salih EY, Mohammed MKA. Er2O3-incorporated SnO2 for fast-response visible-blind UV photodetector: role of Er2O3 in device performance. Mater Chem Phys 2026;348:131656. https://doi.org/10.1016/j.matchemphys.2025.131656.
[24] Ascencio Aguirre FM, Herrera Becerra R. New synthesis of bismuth oxide nanoparticles Bi_2O_3 assisted by tannic acid. Appl Phys A 2015;119:909–15. https://doi.org/10.1007/s00339-015-9039-x.
[25] Ibrahim MK, Mahmood AI, Fandi SK, Rzaij JM. Development of an anthracene-coated SMF-MMF-SMF sensor for low-dose UV radiation detection and dosimetry. Braz J Phys 2025;55:10. https://doi.org/10.1007/s13538-024-01652-2.
[26] Rzaij JM, Khdr Al Attwani NF, Salih EY, Mohammed MKA. Rare-earth Sm2O3-doped SnO2 : tailoring optoelectrical behaviors for a self-driven heterojunction UV-NIR photodetector. Mater Adv 2025;6:6542–9. https://doi.org/10.1039/D5MA00719D.
[27] Kumari L, Lin J-H, Ma Y-R. One-dimensional Bi 2 O 3 nanohooks: synthesis, characterization and optical properties. J Phys Condens Matter 2007;19:406204. https://doi.org/10.1088/0953-8984/19/40/406204.
[28] Oudghiri-Hassani H, Rakass S, Al Wadaani FT, Al-ghamdi KJ, Omer A, Messali M, et al. Synthesis, characterization and photocatalytic activity of α-Bi_2O_3 nanoparticles. J Taibah Univ Sci 2015;9:508–12. https://doi.org/10.1016/j.jtusci.2015.01.009.
[29] Salim ET, Al-Douri Y, Al Wazny MS, Fakhri MA. Optical properties of cauliflower-like Bi_2O_3 nanostructures by reactive pulsed laser deposition (PLD) technique. Sol Energy 2014;107:523–9. https://doi.org/10.1016/j.solener.2014.05.020.
[30] Altowyan AS, Shaban M, Abdelkarem K, El Sayed AM. The impact of Co doping and annealing temperature on the electrochemical performance and structural characteristics of SnO2 nanoparticulate photoanodes. Materials (Basel) 2022;15:6534. https://doi.org/10.3390/ma15196534.
[31] Ahmed HH, Ali AM, Abd AN. (Bi_2O_3) NPs biosynthesis, characterization and using for solar cell application. J Biomech Sci Eng 2023:179–90. https://doi.org/10.17605/OSF.IO/TF5AP.